Title	The Role of Granule Size on the Kinetics of Electrochemical Reduction of SiO2 Granules in Molten CaCl2
Author(s)	Yang, Xiao; Yasuda, Kouji; Nohira, Toshiyuki; Hagiwara, Rika; Homma, Takayuki
Citation	Metallurgical and Materials Transactions B: Process Metallurgy and Materials Processing Science (2016), 47(1): 788-797
Issue Date	2016-02
URL	http://hdl.handle.net/2433/230381
Right	This is a post-peer-review, pre-copyedit version of an article published in 'Metallurgical and Materials Transactions B'. The final authenticated version is available online at: https://doi.org/10.1007/s11663-015-0456-1; The full-text file will be made open to the public on 1 February 2017 in accordance with publisher's 'Terms and Conditions for Self-Archiving'.; This is not the published version. Please cite only the published version. この論文は出版社版でありません。引用の際には出版社版をご確認ご利用ください。
Type	Journal Article
Textversion	author

The Role of Granule Size on the Kinetics of Electrochemical Reduction of SiO_2 Granules in Molten $CaCl_2$

Xiao Yang[a], Kouji Yasuda[b,c], Toshiyuki Nohira[a], Rika Hagiwara[b], and Takayuki Homma[d]

[a]Institute of Advanced Energy, Kyoto University, Gokasho, Uji, Kyoto 611-0011, Japan

[b]Graduate School of Energy Science, Kyoto University, Yoshida-honmachi, Sakyo-ku, Kyoto 606-8501, Japan

[c]Environment, Safety and Health Organization, Kyoto University, Yoshida-honmachi, Sakyo-ku, Kyoto 606-8501, Japan

[d]Faculty of Science and Engineering, Waseda University, 3-4-1 Okubo, Shinjuku-ku, Tokyo 169-8555, Japan

Corresponding authors:

X. Yang (yang.xiao.6a@kyoto-u.ac.jp)

T. Nohira (nohira.toshiyuki.8r@kyoto-u.ac.jp)

Abstract

As a fundamental study to develop a new process for producing solar-grade silicon, the effect of granule size on the kinetics of the electrochemical reduction of SiO_2 granules in molten $CaCl_2$ was investigated. SiO_2 granules with different size ranges were electrolyzed in molten $CaCl_2$ at 1123 K (850 °C). The reduction kinetics was evaluated on the basis of the growth rate of the reduced Si layer and the behavior of the current during electrolysis. The results indicated that finer SiO_2 granules are more favorable for a high reduction rate because the contact resistance between the bottom Si plate and the reduced Si particles is small and the diffusion of O^{2-} ions in $CaCl_2$ inside the porous Si shell is easy. Electrolysis using SiO_2 granules less than 0.1 mm in size maintained a current density of no less than 0.4 A cm^{-2} within 20 min, indicating that the electrochemical reduction of fine SiO_2 granules in molten $CaCl_2$ has the potential of becoming a high-yield production process for solar-grade silicon.

I. INTRODUCTION

The global photovoltaic (PV) market has been growing rapidly in recent years. In 2013, the annual installation of PV systems in the world reached 37 GW,[1] which was a 60-fold increase as compared to 2003. Yet the power globally generated from solar energy was less than 0.5 pct of the total power generation in 2012.[2] According to a study by the German Advisory Council on Global Change (WBGU), solar energy is expected to become a major energy source, reaching 20 pct of the total world energy by 2050 and 70 pct by 2100.[3] Presently, the dominant material for solar cells is silicon, particularly crystalline silicon. Crystalline silicon solar cells represented 90.1 pct of the global production of all types of solar cells in 2013.[4] Because they offers advantages in terms of high conversion efficiency, high durability, non-toxicity, and abundant resources, silicon solar cells are the only candidate to meet the market demand in the future when PV installation could climb to several hundred GW per year.

The increasing demand for PV systems boosts the production of high-purity polycrystalline Si dramatically. The global production of polycrystalline Si in 2013 saw a 10-fold increase since 2003 to 233,800 t,[5] more than 90 pct of which was supplied to the PV industry. Such growth is expected to continue over the long term. For PV applications, the purity of Si must be at least 6N (99.9999 pct), and this product is called solar-grade Si (SOG-Si). The dominant technology for SOG-Si production is the Siemens process,[6-8] which represents approximately 90 pct of the global

50 production. In spite of the ability to produce Si at purity levels above 9N, the Siemens process,
51 which utilizes chemical vapor deposition using trichlorosilane ($SiHCl_3$), requires high energy
52 consumption and results in low productivity. Production of SOG-Si based on pyrolysis of
53 monosilane (SiH_4) in a fluidized bed reactor (FBR) is the main competitor to the Siemens process
54 and represents about 10 pct of the market.[8-10] FBR consumes less energy and it is more economical
55 than the Siemens process, yet limitations in terms of purity control and productivity inhibit its
56 commercial application. Upgrading metallurgical-grade silicon (UMG) is an emerging process for
57 SOG-Si production. The aim of this process is to cost-effectively refine metallurgical-grade Si by
58 slag treatment, acid leaching, and directional solidification.[11-13] However, UMG has a relatively
59 small market share at present because of problems with purity control.[8,14] Various attempts have
60 been made to optimize the present technologies to improve energy efficiency and productivity and to
61 reduce cost.[15-20] Meanwhile, new SOG-Si production processes[21-22] such as the carbothermic
62 reduction of silica using high-purity raw materials,[23] refining of metallurgical-grade Si by different
63 approaches,[24-32] metallothermic reduction of silicon compounds,[33-40] and electrochemical
64 processes,[41-48] are being developed to challenge the existing technologies.

65 Electrochemical reduction of solid oxides in molten salt has been widely studied since it was
66 firstly reported by Fray and his colleagues.[49-57] We originally demonstrated that solid silica (SiO_2)
67 can be electrochemically reduced to solid Si in molten salts via the solid-to-solid reaction: [58-71]

$$SiO_2\ (s) + 4e^- \rightarrow Si\ (s) + 2O^{2-} \quad (1)$$

Similar works have been reported by other researchers.[72-84] Chen and his colleagues[72-75] studied the reduction behavior of SiO_2 plates or pellets in molten $CaCl_2$ based on electrochemical measurements. We came up with a novel idea for SOG-Si production by combining direct electrochemical reduction with the use of high-purity silica, acid leaching, and directional solidification.[64] Impurities in the Si produced by this method were experimentally demonstrated to be at a low level.[68] A semi-continuous electrochemical reduction process was thus proposed,[69] in which SiO_2 granules as the raw material supplied from the top side of the electrolysis cell are reduced at the cathode placed at the bottom and recovered as slurry containing molten $CaCl_2$. The kinetic characteristics of the reducing process of SiO_2 granules were clarified by measuring the weight change of the samples during electrolysis.[70] The apparent current density was 0.7 A cm^{-2} at the initial stage of electrolysis, which indicates the promise of this process in terms of productivity.

An integrated understanding of the mechanism and kinetics of the direct electrochemical reduction of solid SiO_2 in a molten salt is crucial for upscaling of the laboratory experiment to commercial production. In our previous study, we systematically investigated the reduction behavior of SiO_2 granules on a bottom cathode in molten $CaCl_2$ at 1123 K (850 °C) by visually observing changes to the reaction interfaces after different electrolysis durations.[71] The overall reduction was found to

proceed via two different routes: (1) from the SiO_2 granules near the conductor to the distant granules along the granule surfaces and (2) from the surface to the core in each partly reduced granule. Formation of a core (SiO_2)–shell (Si) structure for partly reduced SiO_2 granules indicated that the reduction along the granule surfaces was faster than that from the surface to the core. On the basis of such findings, finer SiO_2 granules are expected to be more favorable for a high reduction rate owing to the larger surface area. However, this expectation needs to be experimentally confirmed.

High productivity is crucial for every practical production process for SOG-Si, including molten salt electrolysis. In this process, the size of SiO_2 granules is considered to be one of the key parameters that strongly affects the reduction kinetics and thus determines the productivity. Therefore, the purpose of the present study was to clarify the effect of granule size on the kinetics of the electrochemical reduction of SiO_2 granules in molten $CaCl_2$. SiO_2 granules with different size ranges were electrolyzed in molten $CaCl_2$ at 1123 K (850 °C). The reduction kinetics was quantitatively evaluated in terms of both the growth rate of the reduced layer and the behavior of the current during electrolysis. A reaction model that illustrates the reduction process and the dependence of reduction kinetics on granule size is proposed.

II. EXPERIMENTAL

A. *Materials and Apparatus*

Approximately 400 g of $CaCl_2$ (Kojundo Chemical Lab. Co., Ltd., 99 pct) was used as the electrolyte bath. Prior to use, the $CaCl_2$ was dried under vacuum at 453 K (180 °C) for 72 h and 773 K (500 °C) for 24 h to remove the residual moisture. Approximately 0.13 g of SiO_2 granules (Kojundo Chemical Lab. Co., Ltd., 99 pct) in four size ranges (less than 0.1 mm, 0.10–0.25 mm, 0.5–1.0 mm, and 1.0–2.0 mm), shown in Figure 1, were used in this study. These granules were obtained from large granules (2.0–5.0 mm) after grinding and screening.

********** Figure 1 **********

Figure 2(a) shows a schematic of the electrolysis cell. An Al_2O_3 crucible (Nikkato Corp., o.d. 90 × i.d. 80 × height 100 mm) charged with $CaCl_2$ was set inside a SiO_2 vessel and heated to 1123 K (850 °C) in a dry Ar atmosphere (100 mL min^{-1}). The working electrode (WE) comprised an Al_2O_3 tube (Nikkato Corp., o.d. 8 × i.d. 5 × height 15 mm) and a Si plate [Nilaco Corp., diameter 10.0 × thickness 0.5 mm, n-type, (100) plane], which served as a container and a current collector respectively, as shown in Figure 2(b). SiO_2 granules were charged in the Al_2O_3 tube. A nickel wire (Nilaco Corp., diameter 1.0 mm, 99 pct) used as the current lead was connected to the Si plate by threading it into a drilled hole (diameter 1.1 mm). With this setup, electrical contact to the SiO_2 occurred only through the Si plate at the bottom of the Al_2O_3 tube.

********** Figure 2 **********

The counter electrode (CE) was a glassy carbon rod (Tokai Carbon Co., Ltd., diameter 5.2 mm). The reference electrode (RE) was an Ag^+/Ag electrode prepared by immersing a silver wire (Nilaco Corp., diameter 1.0 mm, 99 pct) into $CaCl_2$ containing 0.5 mol pct AgCl (Wako Pure Chemical Co., Ltd., 99.5 pct) in a mullite tube (Nikkato Corp., o.d. 6 × i.d. 4 × height 450 mm).[63] A molybdenum wire (Nilaco Corp., diameter 1.0 mm, 99 pct) was used to conduct the cyclic voltammetry to calibrate the Ca^{2+}/Ca potential and check the potential of the Ag^+/Ag reference electrode.

B. *Procedure*

After conducting the cyclic voltammetry using the Mo wire to calibrate the Ca^{2+}/Ca potential, the potential of the working electrode was set at 0.5 V vs. Ca^{2+}/Ca for the potentiostatic electrolysis for 10–100 min. The working electrode was immediately taken out from the melt after electrolysis and a new one was immersed for another run. The post-electrolysis working electrode was cut vertically into two halves to observe the cross section. In some cases, the post-electrolysis working electrode was washed in 10 M HCl (aq.) for 3 h to disassemble the Si plate at the bottom. The upper surface of the Si plate in contact with the SiO_2 granules was observed.

III. RESULTS

A. *Contact of SiO_2 Granules with the Bottom Si Plate*

Figure 3 compares the appearance of the upper surface of the bottom Si plate after electrolysis for 10 min using SiO_2 granules of different size ranges, as well as that of a blank test with no SiO_2 granules. In the case of the blank test [Figure 3(e)], the surface was essentially smooth and integrated. When using SiO_2 granules less than 0.1 mm in size [Figure 3(a)], some parts of the surface were broken, and a large amount of reduced Si, which appears brown in the figure, was attached to the surface. This result indicates that the reduced Si and the bottom Si plate were in close contact with each other during electrolysis. The broken surface was caused by disassembling the Si plate from the post-electrolysis electrode. Since the crystallization rate for amorphous Si increases with increasing temperature and reaches 1 μm s^{-1} at 1123 K (850 °C),[85] the reduced Si, which was amorphous immediately after its formation, might have rapidly crystallized and sintered to have the same orientation as the bottom Si plate. In the case of SiO_2 granules 1.0–2.0 mm in size [Figure 3(d)], only a small amount of reduced Si was found on the surface. In Figures 3(a)–(d), it can be noticed that the quantity of attached Si and broken areas are decreasing and the surface becomes more integrated with increasing SiO_2 granule size. This trend indicates that the contact of SiO_2 granules with the bottom Si plate was improved by decreasing the granule size.

********** Figure 3 **********

B. ***Growth of the Reduced Si Layer***

Figure 4 shows the cross sections of the working electrodes using SiO_2 granules with different

size ranges after electrolysis for (I) 20 min and (II) 60 min at 0.5 V vs. Ca^{2+}/Ca in molten $CaCl_2$ at 1123 K (850 °C). For each sample, a dark brown layer is observed above the Si plate at the bottom. Formation of crystalline Si in this layer was confirmed by X-ray diffraction (XRD) and scanning electron microscopy/energy dispersive X-ray spectroscopy (SEM/EDX). A downward shift of unreduced SiO_2 granules was not observed in Figure 4, indicating that the granules piled on the Si plate as a whole did not apparently shrink downward after reduction. The thickness of the dark layer at three positions in each cross section was measured using a ruler. The average thicknesses of the reduced layers are plotted against electrolysis time in Figure 5. The increased thickness from 20 min to 100 min indicates the propagation of the reduction from the bottom of the SiO_2 layer to the top. Faster growth of the reduced layer was observed for the smaller granules, indicating a larger reduction rate.

********** Figure 4 **********

********** Figure 5 **********

C. *Behavior of the Current*

Figure 6 shows typical current transient curves during electrolysis for 20 min using SiO_2 granules in the various size ranges. The current was larger at the beginning, and it gradually decreased as the electrolysis progressed. A larger current was observed for the smaller granules, indicating a faster reduction rate. Figure 6(e) shows the current of a blank electrolysis test for 10 min using the same

working electrode without a charge of SiO_2 granules. The detected background current is probably due to the side electrochemical reactions of the residual moisture in the molten salt. In this study, the background current was assumed to be independent of the electrolysis time and charge of SiO_2 granules. The effective current corresponding to SiO_2 reduction was considered to be the difference between the measured current and the background current, as indicated in Figure 6.

********** Figure 6 **********

IV. DISCUSSION

A. *Effect of Granule Size on Contact Resistance*

Figure 3 shows that contact between the SiO_2 granules and the bottom Si plate can be improved by decreasing the granule size. Such a difference is schematically illustrated in Figure 7. Assuming the granules are perfectly spherical in shape, the number of contact points equals the number of granules in direct contact with the Si plate (N_I), which can be calculated by

$$N_I = \frac{A_{plate}}{\pi r_0^2} \quad (2)$$

where A_{plate} is the geometrical area of the Si plate and r_0 is the granule radius. Apparently, small granules guarantee a larger number of contact points and thus a greater total contact area as compared with the large granules.

********** Figure 7 **********

As reduction proceeds along the granule surface and from the granule surface to the core, the reduction front gradually moves away from the initial point and spreads along the unreduced part of the SiO_2 granule.[71] The effective potential at the reduction front is determined by the contact resistance between the bottom Si plate and the reduced part of the SiO_2 granules.[73] Because the reduction kinetics is favored at more negative potentials,[61] the usage of small granules guarantees a lower potential drop, thus improving the reduction kinetics.

B. ***Reaction Model for the Reduction during Electrolysis***

Figure 8 illustrates the reduction of the SiO_2 granules piled on the Si plate based on our previous study.[71] A reaction model is proposed to explain the reduction at three stages of electrolysis with the following assumptions: the SiO_2 granules are perfectly spherical in shape; the effective area for each contact point between SiO_2 granule and Si plate is the same and independent of granule size; the granules never expand or shrink during electrolysis; the Si shell formed at the beginning of electrolysis is of an infinitesimal thickness that remains constant over short time periods; the diffusion coefficients of O^{2-} ions in $CaCl_2$ at the granule surface and inside the granule are independent of granule size; partly reduced granules after electrolysis for large time *t* have an identical geometry; and the concentration of O^{2-} ions changes linearly in $CaCl_2$ in the crevices of the Si shells from inside to outside.

********** Figure 8 **********

209 At the start of the electrolysis (infinitesimal time *t*), reduction occurs at the contact points between

210 SiO_2 granules and the Si plate, as shown in Figure 8(a). Since diffusion of O^{2-} ions in $CaCl_2$ is the

211 rate-determining step for the reduction, from Fick's first law of diffusion, the reduction rate at this

212 moment ($\acute{n}_{Si}^{t\to 0}$) can be described by

213 $$\acute{n}_{Si}^{t\to 0} = \frac{\acute{n}_{O^{2-}}^{t\to 0}}{2} = \frac{-1}{2} N_I A_{cont.} D_{surf.} \left(\frac{dC_{O^{2-}}}{dr}\right)_{surf.} = \frac{-A_{plate}}{2\pi {r_0}^2} A_{cont.} D_{surf.} \left(\frac{dC_{O^{2-}}}{dr}\right)_{surf.} \quad (3)$$

214 Where $\acute{n}_{O^{2-}}^{t\to 0}$ is the formation rate of O^{2-} ions at the start of the electrolysis, $A_{cont.}$ is the effective area

215 for each contact point, and $D_{surf.}$ and $\left(\frac{dC_{O^{2-}}}{dr}\right)_{surf.}$ are the diffusion coefficient and concentration

216 gradient of O^{2-} ions in $CaCl_2$ at the granule surface, respectively. Since A_{plate} is constant and $A_{cont.}$,

217 $D_{surf.}$, and $\left(\frac{dC_{O^{2-}}}{dr}\right)_{surf.}$ are considered to be independent of granule size, Eq. [3] indicates that the

218 reduction rate at the start of electrolysis decreases with increasing granule radius.

219 With increasing *t*, reduction proceeds upward along the granule surface and from surface to core

220 with the formation of a Si shell, as shown in Figure 8(b-1). The overall reduction rate ($\acute{n}_{Si}^{overall}$) can

221 be expressed as

222 $$\acute{n}_{Si}^{overall} = \acute{n}_{Si}^{surf.} + \acute{n}_{Si}^{ins.} \approx \acute{n}_{Si}^{surf.} \quad (4)$$

223 where $\acute{n}_{Si}^{surf.}$ and $\acute{n}_{Si}^{ins.}$ are the reduction rate along the surface and from the surface to the core,

224 respectively. Since the reduction from the surface to the core is much slower than the reduction

225 along the surface after electrolysis of small time *t*, only the latter is considered. As illustrated in

226 Figure 8(b-2), the Si shell with a thickness of δ and the center of the granule form a spherical sector

ACD, the cone angle of which is $2\theta\left(0<\theta<\frac{\pi}{2}\right)$. The area of the reduction interface$\left(A_{inter.}^{small t}\right)$ can be calculated as the difference of the lateral area between the spherical sectors ACD and ABE.

$$A_{inter.}^{small\ t}=\pi r_0^2 sin\theta-\pi(r_0-\delta)^2 sin\theta=\pi[r_0^2-(r_0-\delta)^2]sin\theta \quad (5)$$

The reduction rate at small t $\left(\acute{n}_{Si}^{small\ t}\right)$can be described as

$$\acute{n}_{Si}^{small\ t}=\frac{\acute{n}_{O^{2-}}^{small\ t}}{2}=\frac{-N_I\pi}{2}[r_0^2-(r_0-\delta)^2]sin\theta\cdot D_{surf.}\left(\frac{dC_{O^{2-}}}{dr}\right)_{surf.} \quad (6)$$

where $\acute{n}_{O^{2-}}^{small\ t}$ is the formation rate of O^{2-} ions after electrolysis of small time t. Since the volume difference between the spherical sectors ACD and ABE is regarded as the volume of the reduced part of a single SiO_2 granule ($\Delta V_{SiO_2}^{small\ t}$), given as

$$\Delta V_{SiO_2}^{small\ t}=\frac{2}{3}\pi r_0^3(1-cos\theta)-\frac{2}{3}\pi(r_0-\delta)^3(1-cos\theta)=\frac{2}{3}\pi[r_0^3-(r_0-\delta)^3](1-cos\theta) \quad (7)$$

the reduction rate can also be calculated by

$$\acute{n}_{Si}^{small\ t}=\frac{dn_{Si}}{dt}=\frac{d\frac{\rho_{SiO_2}N_I\Delta V_{SiO_2}^{small\ t}}{M_{SiO_2}}}{dt}=\frac{2\rho_{SiO_2}N_I\pi d\{[r_0^3-(r_0-\delta)^3](1-cos\theta)\}}{3M_{SiO_2}dt}$$

$$=\frac{2\rho_{SiO_2}N_I\pi}{3M_{SiO_2}}[r_0^3-(r_0-\delta)^3]sin\theta\frac{d\theta}{dt} \quad (8)$$

where n_{Si} is the number of moles of the reduced Si, $\rho_{SiO_2}$and $M_{SiO_2}$are the density and molar weight of SiO_2, respectively. Combining Eqs. [6] and [8] gives

$$\frac{d\theta}{dt}=\frac{-3M_{SiO_2}[2r_0-\delta]}{4\rho_{SiO_2}[3r_0^2-3r_0\delta+\delta^2]}D_{surf.}\left(\frac{dC_{O^{2-}}}{dr}\right)_{surf.}\approx-\frac{M_{SiO_2}}{2\rho_{SiO_2}r_0}D_{surf.}\left(\frac{dC_{O^{2-}}}{dr}\right)_{surf.} \quad (9)$$

The solution of Eq. [9] with the boundary condition θ= 0 when t = 0 gives

$$\theta=\frac{-M_{SiO_2}t}{2\rho_{SiO_2}r_0}D_{surf.}\left(\frac{dC_{O^{2-}}}{dr}\right)_{surf.} \quad (10)$$

The substitution of Eq. [10] into Eq. [6] gives

$$\acute{n}_{O^{2-}}^{small\ t} = -\frac{A_{plate}}{r_0^2}[2r_0\delta - \delta^2]sin\left[\frac{-M_{SiO_2}t}{2\rho_{SiO_2}r_0}D_{surf.}\left(\frac{dC_{O^{2-}}}{dr}\right)_{surf.}\right]\cdot D_{surf.}\left(\frac{dC_{O^{2-}}}{dr}\right)_{surf.}$$

$$\approx -\frac{2\delta A_{plate}D_{surf.}\left(\frac{dC_{O^{2-}}}{dr}\right)_{surf.}}{r_0}sin\left[\frac{-M_{SiO_2}t}{2\rho_{SiO_2}r_0}D_{surf.}\left(\frac{dC_{O^{2-}}}{dr}\right)_{surf.}\right] \quad (11)$$

Equation [11] clearly indicates that reduction rate after electrolysis of small time *t* decreases with increasing granule radius. It is also understood from Eq. [11] that the reduction rate at the beginning of electrolysis would increase with increasing time *t*. Even though this tendency is not clearly observed in the current experiments because the amount of SiO_2 granules is too small (0.13 g), it was presented in previous experiments on a larger scale (more than 10 g of SiO_2 granules).[69]

After electrolysis of large time *t*, a core (SiO_2)–shell (Si) structure forms for all granules, as shown in Figure 8(c-1). At this moment, the whole granule surface is reduced, and thus only the reduction from the surface to the core continues. The reaction interface is the surface of the unreacted SiO_2 core. The reduction rate ($\acute{n}_{Si}^{large\ t}$) can be calculated as

$$\acute{n}_{Si}^{large\ t} = \frac{\acute{n}_{O^{2-}}^{large\ t}}{2} = -2\pi r_i^2 N_{II} D_{ins.}\left(\frac{dC_{O^{2-}}}{dr}\right)_{ins.} \quad (12)$$

where $\acute{n}_{O^{2-}}^{large\ t}$ is the formation rate of O^{2-} ions after electrolysis of large time *t*, r_i is the radius of the unreduced SiO_2 core as shown in Figure 8(c-2), N_{II} is the number of granules reduced after large time *t*, and $D_{ins.}$ and $\left(\frac{dC_{O^{2-}}}{dr}\right)_{ins.}$ are the diffusion coefficient and concentration gradient of O^{2-} ions in $CaCl_2$ in the crevices of the porous Si shells, respectively. Assuming a linear concentration gradient of O^{2-} ions, $\left(\frac{dC_{O^{2-}}}{dr}\right)_{ins.} = \frac{C_0 - C_i}{r_0 - r_i}$, where C_0 and C_i are the concentrations of O^{2-} ions at the outer and inner surfaces of the Si shell, respectively, Eq. [12] becomes

$$\acute{n}_{Si}^{large\ t} = 2\pi r_i^2 N_{II} D_{ins.} \frac{C_i - C_0}{r_0 - r_i} \quad (13)$$

Since the volume of the reduced part of a single SiO_2 granule ($\Delta V_{SiO_2}^{large\ t}$) can be calculated as

$$\Delta V_{SiO_2}^{large\ t} = \frac{4}{3}\pi r_0^3 - \frac{4}{3}\pi r_i^3 \quad (14)$$

the reduction rate can also be described by

$$\acute{n}_{Si}^{large\ t} = \frac{dn_{Si}}{dt} = \frac{d\frac{\rho_{SiO_2} N_{II} \Delta V_{SiO_2}^{large\ t}}{M_{SiO_2}}}{dt} = \frac{-4\rho_{SiO_2} N_{II} \pi r_i^2}{M_{SiO_2}} \frac{dr_i}{dt} \quad (15)$$

Combining Eqs. [13] and [15] yields

$$\frac{2(r_i - r_0)dr_i}{dt} = \frac{(C_i - C_0) D_{ins.} M_{SiO_2}}{\rho_{SiO_2}} \quad (16)$$

Assuming $D_{ins.}$, C_0, and C_i are independent of time, the solution of Eq. [16] with the boundary condition $r_i = r_0$ when $t = 0$ gives

$$(r_0 - r_i)^2 = \frac{(C_i - C_0) D_{ins.} M_{SiO_2}}{\rho_{SiO_2}} t \quad (17)$$

Since the granule number can be described as

$$N_{II} = \frac{\frac{W_{SiO_2}}{\rho_{SiO_2}}}{\frac{4}{3}\pi r_0^3} = \frac{3W_{SiO_2}}{4\rho_{SiO_2}\pi r_0^3} \quad (18)$$

where W_{SiO_2} is the total weight of SiO_2, the substitution of Eqs. [17] and [18] into Eq. [13] yields

$$\acute{n}_{Si}^{large\ t} = \left[r_0 - \sqrt{\frac{(C_i - C_0) D_{ins.} M_{SiO_2}}{\rho_{SiO_2}} t}\right]^2 \frac{3W_{SiO_2}}{2r_0^3} \sqrt{\frac{(C_i - C_0) D_{ins.}}{M_{SiO_2} \rho_{SiO_2} t}} \quad (19)$$

Equation [19] is a monotonically decreasing function of r_0, which indicates that the reduction rate at an electrolysis time of large t decreases with increasing granule radius. Moreover, the reduction rate also decreases with increasing electrolysis time. These tendencies are in accordance with the experimental results shown in Figure 6.

C. *Apparent Current Density*

Based on the current transient curves during electrolysis (Figure 6), the apparent current density was evaluated. In the case of the blank test without charging with SiO_2 granules, only the current (I_{blank}) contributed by the side electrochemical reactions (I_{side}) is obtained

$$I_{blank} = I_{side} \tag{20}$$

For the electrolysis after charging with SiO_2 granules, the overall current (I_{all}) is the result of both the SiO_2 reduction (I_{SiO_2}) and the side reactions.

$$I_{all} = I_{SiO_2} + I_{side} \tag{21}$$

Assuming the current corresponding to side reactions is independent of the electrolysis time and charge of SiO_2 granules, the apparent current density corresponding to SiO_2 reduction (i_{SiO_2}) can be calculated by

$$i_{SiO_2} = \frac{I_{SiO_2}}{A_{plate}} = \frac{I_{all} - I_{blank}}{A_{plate}} \tag{22}$$

Using the data in Figure 6 and taking $I_{side} \equiv 0.05A$, the apparent current densities during electrolysis for 20 min using SiO_2 granules with various size ranges were calculated and the results are shown in Figure 9. It is clear that the current density gradually decreases with increasing electrolysis time and that smaller SiO_2 granules results in a larger current density. In the case of using SiO_2 granules less than 0.1 mm in size, electrolysis within 20 min maintained a current density of no less than 0.4 A cm^{-2}. This result basically agrees with those of a previous study, in which the

297 current density was obtained by calculating from the weight change of the sample before and after
298 electrolysis.[70] These results indicate that the productivity would be improved by using fine SiO_2
299 granules as the raw materials for a new SOG-Si production process in the future.

300 ********** Figure 9 **********

301

302 **IV. CONCLUSIONS**

303 The effect of granule size on the kinetics of electrochemical reduction of SiO_2 granules in molten
304 $CaCl_2$ at 1123 K (850 °C) was clarified. Fine SiO_2 granules are favorable for a high reduction rate by
305 lowering the contact potential drop between the bottom Si plate and the reduced Si. The use of fine
306 granules also improves the diffusion of O^{2-} ions in $CaCl_2$ inside the porous Si shell formed on the
307 SiO_2 core. The electrolysis using SiO_2 granules less than 0.1 mm in size maintained a current density
308 of no less than 0.4 A cm^{-2} within 20 min, indicating that electrochemical reduction of fine SiO_2
309 granules in molten $CaCl_2$ has the potential to become a high-yield solar-grade silicon production
310 process.

311 **ACKNOWLEDGMENTS**

312 This study was partly supported by Core Research for Evolutionary Science and Technology

(CREST), Japan Science and Technology Agency (JST) and Grants-in-Aid for Scientific Research A from the Japan Society for the Promotion of Science (JSPS).

NOMENCLATURE

$A_{\text{cont.}}$	Effective area for each contact point between SiO_2 granules and the Si plate
A_{plate}	Geometrical area of the bottom Si plate
$A_{inter.}^{small\ t}$	Area of the reduction interface after electrolysis of small time *t*
C_{i}	Concentration of O^{2-} ions at the inner surface of the Si shell of the partly reduced SiO_2 granules after electrolysis of large time *t*
C_0	Concentration of O^{2-} ions at the outer surface of the Si shell of the partly reduced SiO_2 granules after electrolysis of large time *t*
$D_{\text{ins.}}$	Diffusion coefficient of O^{2-} ions in $CaCl_2$ in the crevice of the porous Si shell of the partly reduced SiO_2 granules after electrolysis of large time *t*
$D_{\text{surf.}}$	Diffusion coefficient of O^{2-} ions in $CaCl_2$ at the SiO_2 granule surface
$\left(\frac{dC_{O^{2-}}}{dr}\right)_{ins.}$	Concentration gradient of O^{2-} ions in $CaCl_2$ in the crevice of the porous Si shell of the partly reduced SiO_2 granules after electrolysis of large time *t*
$\left(\frac{dC_{O^{2-}}}{dr}\right)_{surf.}$	Concentration gradient of O^{2-} ions in $CaCl_2$ at the SiO_2 granule surface
I_{all}	Current obtained in the case of a test with charging SiO_2
I_{blank}	Current obtained in the case of a blank test without charging SiO_2
I_{side}	Current contributed by the side electrochemical reactions
I_{SiO_2}	Current contributed by SiO_2 reduction
i_{SiO_2}	Apparent current density corresponding to SiO_2 reduction
M_{SiO_2}	Molar weight of SiO_2
N_{I}	Number of SiO_2 granules directly neighboring the Si plate
N_{II}	Total number of SiO_2 granules
n_{Si}	Number of moles of the reduced Si
$\acute{n}_{Si}^{t\to 0}$	Reduction rate of SiO_2 granules at the start moment of the electrolysis
$\acute{n}_{Si}^{overall}$	Overall reduction rate of SiO_2 granules
$\acute{n}_{Si}^{surf.}$	Reduction rate of SiO_2 granules along surface
$\acute{n}_{Si}^{ins.}$	Reduction rate of SiO_2 granules from surface to core
$\acute{n}_{Si}^{small\ t}$	Reduction rate of SiO_2 granules after electrolysis of small time *t*
$\acute{n}_{Si}^{large\ t}$	Reduction rate of SiO_2 granules after electrolysis of large time *t*
$\acute{n}_{O^{2-}}^{t\to 0}$	Formation rate of O^{2-} ions at the start moment of the electrolysis
$\acute{n}_{O^{2-}}^{small\ t}$	Formation rate of O^{2-} ions after electrolysis of small time *t*
$\acute{n}_{O^{2-}}^{large\ t}$	Formation rate of O^{2-} ions after electrolysis of large time *t*
r_0	Radius of the SiO_2 granule in Figure 8(b-2)
r_{i}	Radius of the unreduced core of the partly reduced SiO_2 granule in Figure 8(c-2)
t	Electrolysis time
$\Delta V_{SiO_2}^{small\ t}$	Volume of the reduced part of a SiO_2 granule after electrolysis of small time *t*
	Volume of the reduced part of a SiO_2 granule after electrolysis of large time *t*
	Total weight of SiO_2 granules
	Thickness of the reduced Si shell after electrolysis of small time *t* in Figure 8(b-2)

$\Delta V_{SiO_2}^{large\ t}$	Half of the cone angle of the spherical sector ACD in Figure 8(b-2)
W_{SiO_2}	Density of SiO_2
δ	
θ	
ρ_{SiO_2}	

REFERENCES

1. European Photovoltaic Industry Association: *Market Report 2013*, European Photovoltaic Industry Association, Brussels, March, 2014.

2. Observ'ER: *Fifteenth Inventory 2013 Edition–Worldwide Electricity Production from Renewable Energy Sources*, Observ'ER, Paris, June, 2013.

3. German Advisory Council on Global Change: *World in Transition–Towards Sustainable Energy Systems*, Earthscan, London, 2003.

4. Arumu Publishing Co.: *Rare Metal News*, Arumu Publishing Co., Tokyo, August, 2014.

5. Arumu Publishing Co.: *Rare Metal News*, Arumu Publishing Co., Tokyo, April, 2014.

6. H. Schweickert, K. Reuschel, and H. Gutsche: U.S. patent, US3,011,877, 1961.

7. H. Gutsche: U.S. patent, US3,042,494, 1962.

8. G. Bye and B. Ceccaroli: *Sol. Energy Mater. Sol. Cells*, 2014, vol. 130, pp.634-46.

9. H. W. Ling: U.S. Patent, US3,012,861, 1961.

10. L. Bertrand, N. Star, and C. M. Olson: U.S. Patent, US3,012,862, 1961.

11. K. Morita and T. Miki: *Intermetallics*, 2003, vol. 11, pp. 1111–17.

12. V. Hoffmann, K. Petter, J. Djordjevic-Reiss, E. Enebakk, J. T. Håkedal, R. Tronstad, T. Vlasenko, I. Buchovskaja, S. Beringov, and M. Bauer: *Proc. 23rd EU PVSEC*, Valencia, Spain, 1-5 Sept. 2008, pp. 1117–20.

13. Y. V. Meteleva-Fischer, Y. Yang, R. Boom, B. Kraaijveld and H. Kuntzel: *JOM*, 2012, vol. 64, pp. 957–967.

14. IHS Technology: *PV Manufacturing Technology Report - 2014*, IHS Technology, El Segundo Feb., 2014.

15. S. Wakamatsu and H. Oda: PCT International Patent, WO2001/085613, 2001.

16. A. Søiland, M. G. Dolmen, J. Heide, U. Thisted, G. Halvorsen, G. Ausland, K. Friestad, P. Preis, K. Peter, O. Graf, T. Bartel, and R. Tronstad: *Sol. Energy Mater. Sol. Cells*, 2014, vol. 130, pp. 661-67.

17. K. Yasuda, K. Morita, and T. H. Okabe: *Energy Technology*, 2014, vol. 2, pp. 141–54.

18. W. O. Filtvedt, M. Javidi, A. Holt, M. C. Melaaen, E. Marstein, H. Tathgar, and P. A. Ramachandran: *Sol. Energy Mater. Sol. Cells*, 2010, vol. 94, pp. 1980–95.

19. B. G. Gribov and K. V. Zinov'ev: *Inorg. Mater.*, 2003, vol. 39, pp. 653–62.

20. H. Oda: *Kogyo Zairyo*, 2007, vol. 55, pp. 30–34.

21. A. F. B. Braga, S. P. Moreira, P. R. Zampieri, J. M. G. Bacchin, and P. R. Mei: *Sol. Energy*

Mater. Sol. Cells, 2008, vol. 92, pp. 418–24.

22. M. D. Johnston, L. T. Khajavi, M. Li, S. Sokhanvaran, and M. Barati, *JOM*, 2012, vol. 64, pp. 935–45.

23. Y. Sakaguchi, M. Ishizaki, T. Kawahara, M. Fukai, M. Yoshiyagawa, and F. Aratani, *ISIJ Int.*, 1992, vol. 32, pp. 643–49.

24. K. Suzuki, T. Kumagai, and N. Sano: *ISIJ Int.*, 1992, vol. 32, pp. 630–34.

25. T. Ikeda and M. Maeda: *ISIJ Int.*, 1992, vol. 32, pp. 635–42.

26. J. C. S. Pires, J. Otubo, A. F. B. Braga, and P. R. Mei: *J. Mater. Processing Tech.* 2005, vol. 169, pp. 16–20.

27. J. L. Gumaste, B. C. Mohanty, R. K. Galgali, U. Syamaprasad, B. Nayak, S. K. Singh, and P. K. Jena: *Sol. Energy Mater.*, 1987, vol. 16, pp. 289–96.

28. T. Yoshikawa and K. Morita: *JOM*, 2012, vol. 64, pp. 946–51.

29. I. C. Santos, A. P. Goncalves, C. S. Santos, M. Almeida, M. H. Afonso, and M. J. Cruz: *Hydrometallurgy*, 1990, vol. 23, pp. 237–246.

30. Y. Sun, Q. Ye, C. Guo, H. Chen, X. Lang, F. David, Q. Luo, and C. Yang: *Hydrometallurgy*, 2013, vol. 139, pp. 64–72.

31. J. Safarian and M. Tangstad: *Metall. Mater. Trans. B*, 2012, vol. 43, pp. 1427–45.

32. M. A. Martorano, J. B. F. Neto, T. S. Oliveira, and T. O. Tsubaki: *Mater. Sci. Eng. B*, 2011, vol.

176, pp. 217–26.

33. S. Honda, M. Yasueda, S. Hayashida, and M. Yamaguchi: Japanese Patent Application, JP2007145663, 2007.

34. K. Saegusa and T. Yamabayashi: PCT International Patent WO2007/001093, 2007.

35. K. Yasuda and T. H. Okabe: *JOM*, 2010, vol. 62, pp 94–101.

36. K. Yasuda, K. Saegusa, and T. H. Okabe: *Metall. Mater. Trans. B*, 2011, vol. 42, pp. 37–49.

37. E. Robert and T. Zijlema: PCT International Patent WO2006/100114, 2006.

38. C. Rosenkilde: PCT International Patent WO2008/120994, 2008.

39. H. Tezuka: PCT International Patent WO2008/153181, 2008.

40. K. Saito, H. Munakata, and T. Mizoguchi: PCT International Patent WO2011/071030, 2011.

41. R. Monnier, D. Barakat, and J. Giacometti: U.S. Patent, US3,254,010, 1966.

42. J. Olson and K. Carleton: *J. Electrochem. Soc.*, 1981, vol. 128, pp. 2698–99.

43. J. Cai, X. Luo, G. M. Haarberg, O. E. Kongstein, and S. Wang: *J. Electrochem. Soc.*, 2012, vol. 159, pp. D155–58.

44. D. Elwell and R. S. Feigelson: *Sol. Energy Mater.*, 1982, vol. 6, pp. 123–45.

45. D. Elwell and G. M. Rao: *J. Appl. Electrochem.*, 1988, vol. 18, pp. 15–22.

46. T. Oishi, M. Watanabe, K. Koyama, M. Tanaka, and K. Saegusa: *J. Electrochem. Soc.*, 2011, vol. 158, pp. E93–99.

47. J. Xu and G. M. Haarberg: *High Temperature Materials and Processes*, 2013, vol. 32, pp. 97–105.

48. Y. Jiang, J. Xu, X. Guan, U.B. Pal, and S.N. Basu: *MRS Proceedings*, 2013, vol. 1493, pp. 231–35.

49. G. Z. Chen, D. J. Fray, and T. W. Farthing: *Nat.*, 2000, vol. 407, pp. 361-64.

50. X. Y. Yan and D. J. Fray: *Metall. Mater. Trans. B*, 2002, vol. 33, pp. 685–93.

51. G. Z. Chen, E. Gordo, and D. J. Fray: *Metall. Mater. Trans. B*, 2004, vol. 35, pp. 223–33.

52. K. S. Mohandas and D. J. Fray: *Metall. Mater. Trans. B*, 2009, vol. 40, pp. 685–99.

53. X. Y. Yan and D. J. Fray: *J. Appl. Electrochem.*, 2009, vol. 39, pp. 1349–60.

54. Q. Song, Q. Xu, X. Kang, J. Du, and Z. Xi: *J. Alloy. Compd.*, 2010, vol. 490, pp. 241–46.

55. M. Erdoğan and I. Karakaya: *Metall. Mater. Trans. B*, 2010, vol. 41, pp. 798–804.

56. A. M. Abdelkader and D. J. Fray: *Electrochim. Acta*, 2012, vol. 64, pp. 10-16.

57. W. Xiao and D. Wang: *Chem. Soc. Rev.*, 2014, vol. 43, pp. 3215-28.

58. T. Nohira, K. Yasuda, and Y. Ito: *Nat. Mater.*, 2003, vol. 2, pp. 397–401.

59. K. Yasuda, T. Nohira, K. Amezawa, Y. H. Ogata, and Y. Ito: *J. Electrochem. Soc.*, 2005, vol. 152, pp. D69–74.

60. K. Yasuda, T. Nohira, Y. H. Ogata, and Y. Ito: *Electrochim. Acta*, 2005, vol. 51, pp. 561–65.

61. K. Yasuda, T. Nohira, and Y. Ito: *J. Phys. Chem. Solids*, 2005, vol. 66, pp. 443–47.

62. K. Yasuda, T. Nohira, Y. H. Ogata, and Y. Ito: *J. Electrochem. Soc.*, 2005, vol. 152, pp. D208–12.

63. K. Yasuda, T. Nohira, R. Hagiwara, and Y. H. Ogata: *J. Electrochem. Soc.*, 2007, vol. 154, pp. E95–E101.

64. K. Yasuda, T. Nohira, R. Hagiwara, and Y. H. Ogata: *Electrochim. Acta,*. 2007, vol. 53, pp. 106–10.

65. K. Yasuda, T. Nohira, K. Takahashi, R. Hagiwara, and Y. H. Ogata: *J. Electrochem. Soc.*, 2005, vol. 152, pp. D232–37.

66. Y. Nishimura, T. Nohira, K. Yasuda, Y. Fukunaka, and R. Hagiwara: *Trans. Mater. Res. Soc. Jpn.*, 2010, vol. 35, pp. 47-49.

67. Y. Nishimura, T. Nohira, K. Kobayashi, and R. Hagiwara: *J. Electrochem. Soc.*, 2011, vol.158, pp. E55–59.

68. K. Yasuda, T. Nohira, K. Kobayashi, N. Kani, T. Tsuda, and R. Hagiwara: *Energy Technology*, 2013, vol. 1, pp. 245–52.

69. T. Toba, K. Yasuda, T. Nohira, X. Yang, R. Hagiwara, K. Ichitsubo, K. Masuda, and T. Homma: *Electrochemistry*, 2013, vol. 81, pp. 559–65.

70. X. Yang, K. Yasuda, T. Nohira, R. Hagiwara, and T. Homma: *J. Electrochem. Soc.*, 2014, vol. 161, pp. D3116–19.

71. X. Yang, K. Yasuda, T. Nohira, R. Hagiwara, and T. Homma: *Metall. Mater. Trans. B*, 2014, vol. 45, pp. 1337-44.

72. X. Jin, P. Gao, D. Wang, X. Hu, and G. Z. Chen: *Angew. Chem.*, 2004, vol. 116, pp. 751–54.

73. W. Xiao, X. Jin, Y. Deng, D. Wang, X. Hu, and G. Z. Chen: *ChemPhysChem.*, 2006, vol. 7, pp. 1750–58.

74. W. Xiao, X. Jin, Y. Deng, D. Wang, X. Hu, and G. Z. Chen: *J. Electroanal. Chem.*, 2010, vol. 639, pp. 130–40.

75. W. Xiao, X. Jin, and G. Z. Chen: *J. Mater. Chem. A.*, 2013, vol. 1, pp. 10243–50.

76. W. Xiao, X. Wang, H. Yin, H. Zhu, X. Mao, and D. Wang: *RSC Advances*, 2012, vol. 2, pp. 7588–93.

77. P. C. Pistorius and D. J. Fray: *J. S. Afr. Inst. Min. Metall.*, 2006, vol. 106, pp. 31–41.

78. S. Lee, J. Hur, and C. Seo: *J. Ind. Eng. Chem.*, 2008, vol. 14, pp. 651–54.

79. E. Juzeliunas, A. Cox, and D. J. Fray: *Electrochem. Comm.*, 2010, vol. 12, pp. 1270–74.

80. E. Ergül, İ. Karakaya, and M. Erdoğan: *J. Alloy. Compd.*, 2011, vol. 509, pp. 899–903.

81. S. K. Cho, F. F. Fan, and A. J. Bard: *Electrochim. Acta*, 2012, vol. 65, pp. 57–63.

82. J. Zhao, S. Lu, L. Hu, and C. Li: *J. Energy Chem.*, 2013, vol. 22, pp. 819-25.

83. J. Zhao, J. Li, P. Ying, W. Zhang, L. Meng, and C. Li: *ChemCom.*, 2013, vol. 49, pp. 4477-79.

84. H. Nishihara, T. Suzuki, H. Itoi, B. An, S. Iwamura, R. Berenguer, and T. Kyotani: *Nanoscale*,

2014, vol. 6, pp. 10574-83.

85. G. Olson and J. Roth: *Mater. Sci. Rep.*, 1988, vol. 3, pp. 1-77.

Caption list

Figure 1—Appearances of the SiO_2 granules with size ranges of (a) less than 0.1 mm, (b) 0.10–0.25 mm, (c) 0.5–1.0 mm and (d) 1.0–2.0 mm.

Figure 2—A schematic of (a) the electrolysis cell and (b) the working electrode.

Figure 3—Appearances of the upper surface of the bottom Si plate after electrolysis using SiO_2 granules with size ranges of (a) less than 0.1 mm, (b) 0.10–0.25 mm, (c) 0.5–1.0 mm, (d) 1.0–2.0 mm for 10 min and (e) a blank electrolysis test for 10 min at 0.5 V vs. Ca^{2+}/Ca in molten $CaCl_2$ at 1123 K (850 °C).

Figure 4—Cross sections of the working electrodes using SiO_2 granules with size ranges of (a) less than 0.1 mm, (b) 0.10–0.25 mm, (c) 0.5–1.0 mm and (d) 1.0–2.0 mm after electrolysis for (I) 20 min and (II) 60 min at 0.5 V vs. Ca^{2+}/Ca in molten $CaCl_2$ at 1123 K (850 °C).

Figure 5—Thickness of the reduced layers after electrolysis for 20, 60 and 100 min using SiO_2 granules with different size ranges at 0.5 V vs. Ca^{2+}/Ca in molten $CaCl_2$ at 1123 K (850 °C).

Figure 6—Current transient curves during electrolysis using SiO_2 granules with size ranges of (a) less than 0.1 mm, (b) 0.10–0.25 mm, (c) 0.5–1.0 mm and (d) 1.0–2.0 mm for 20 min and (e) during a blank electrolysis test for 10 min at 0.5 V vs. Ca^{2+}/Ca in molten $CaCl_2$ at 1123 K (850 °C).

Figure 7—Schematics of the contact between SiO_2 granules and the bottom current collector (Si plate).

Figure 8—Schematics of the reduction of the SiO_2 granules during electrolysis.

Figure 9—Variation of apparent current density during electrolysis within 20 min using SiO_2 granules with size ranges of (a) less than 0.1 mm, (b) 0.10–0.25 mm, (c) 0.5–1.0 mm and (d) 1.0–2.0 mm at 0.5 V vs. Ca^{2+}/Ca in molten $CaCl_2$ at 1123 K (850 °C).

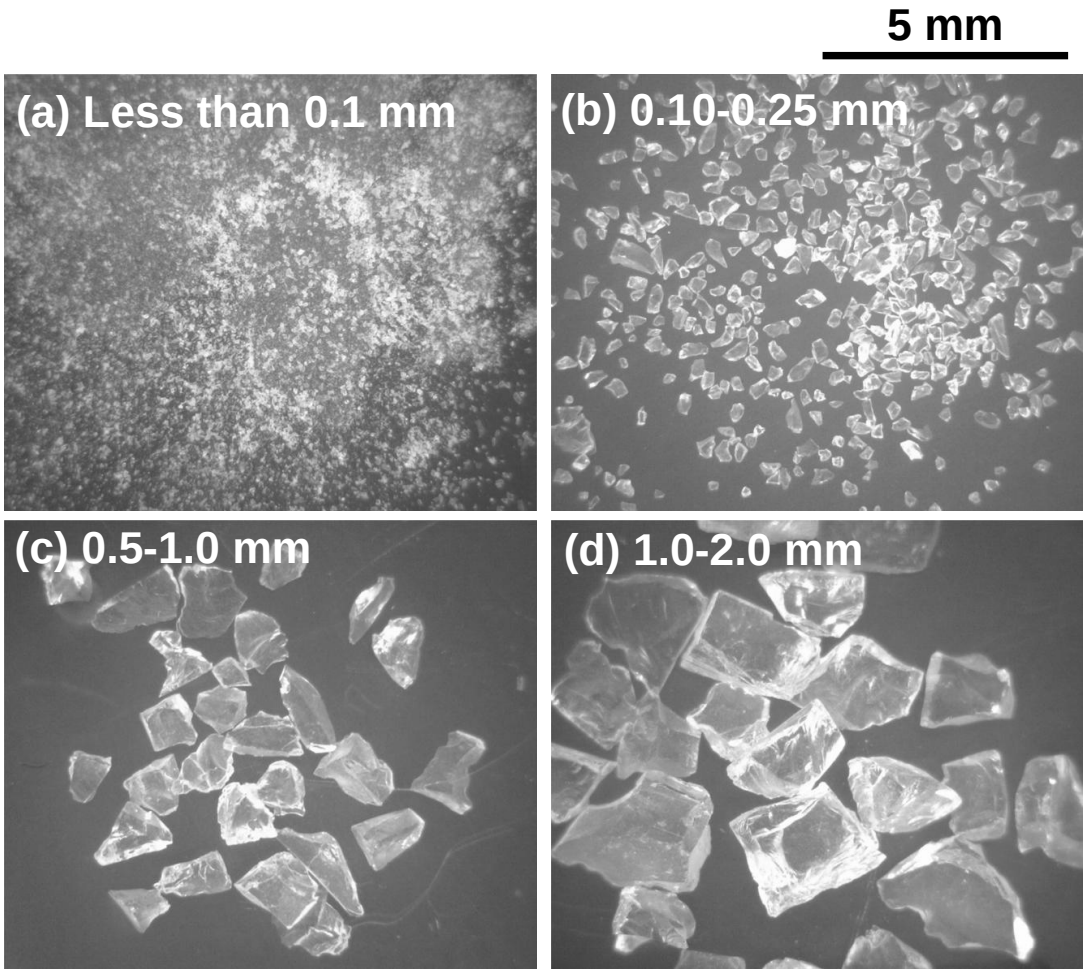

Figure 1—Appearances of the SiO_2 granules with size ranges of (a) less than 0.1 mm, (b) 0.10–0.25 mm, (c) 0.5–1.0 mm and (d) 1.0–2.0 mm.

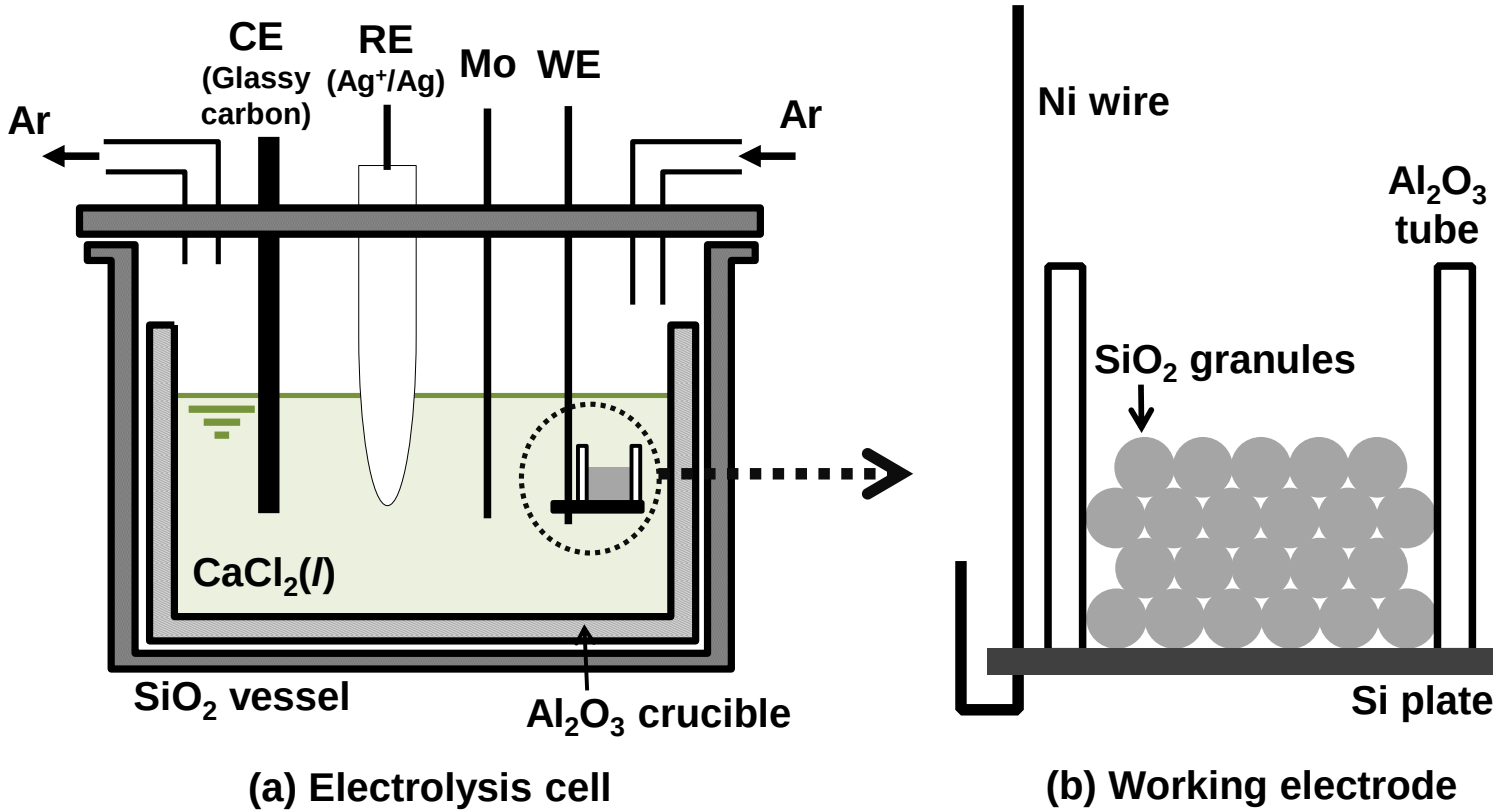

Figure 2—A schematic of (a) the electrolysis cell and (b) the working electrode.

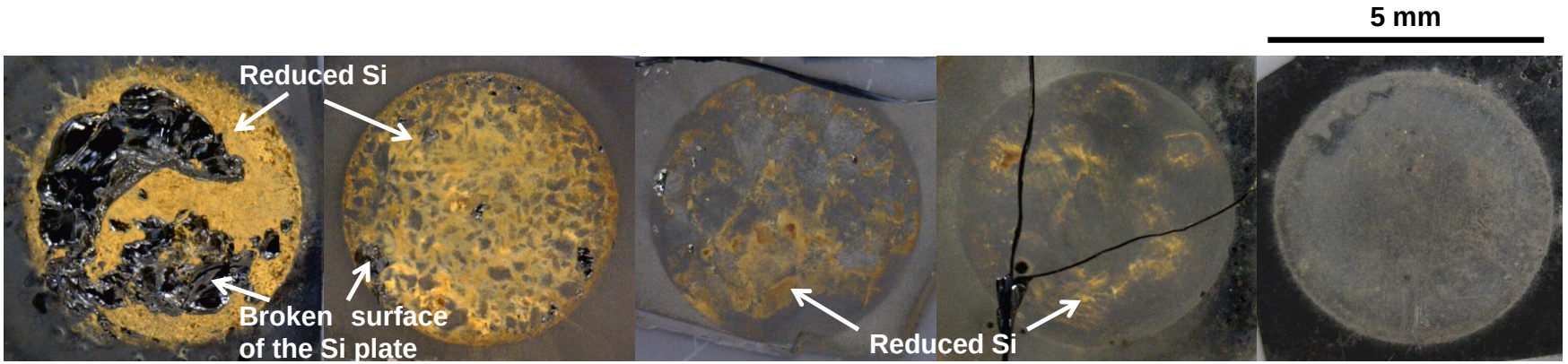

Figure 3—Appearances of the upper surface of the bottom Si plate after electrolysis using SiO_2 granules with size ranges of (a) less than 0.1 mm, (b) 0.10–0.25 mm, (c) 0.5–1.0 mm, (d) 1.0–2.0 mm for 10 min and (e) a blank electrolysis test for 10 min at 0.5 V vs. Ca^{2+}/Ca in molten $CaCl_2$ at 1123 K (850 ℃).

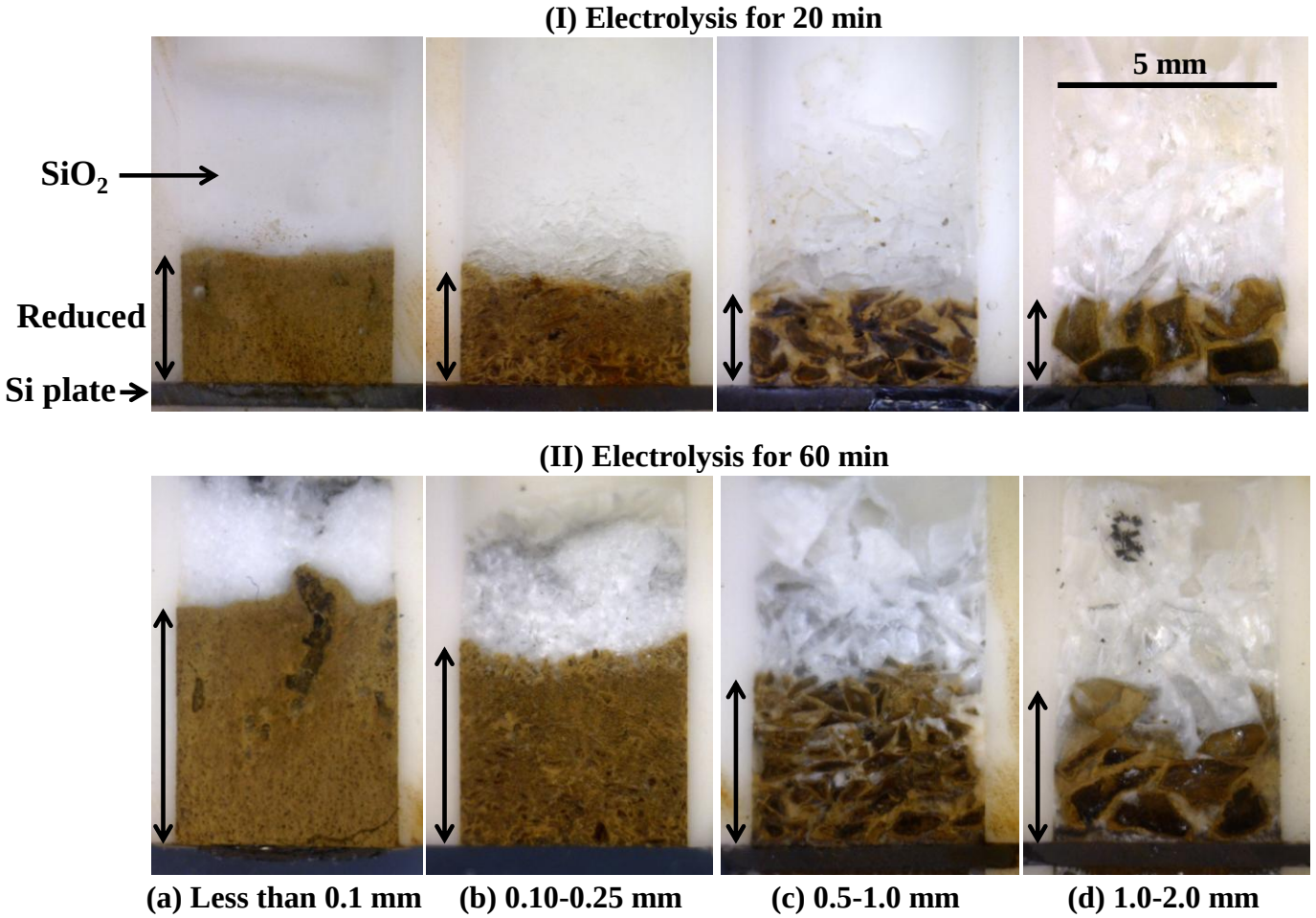

Figure 4—Cross sections of the working electrodes using SiO_2 granules with size ranges of (a) less than 0.1 mm, (b) 0.10–0.25 mm, (c) 0.5–1.0 mm and (d) 1.0–2.0 mm after electrolysis for (I) 20 min and (II) 60 min at 0.5 V vs. Ca^{2+}/Ca in molten $CaCl_2$ at 1123 K (850 ℃).

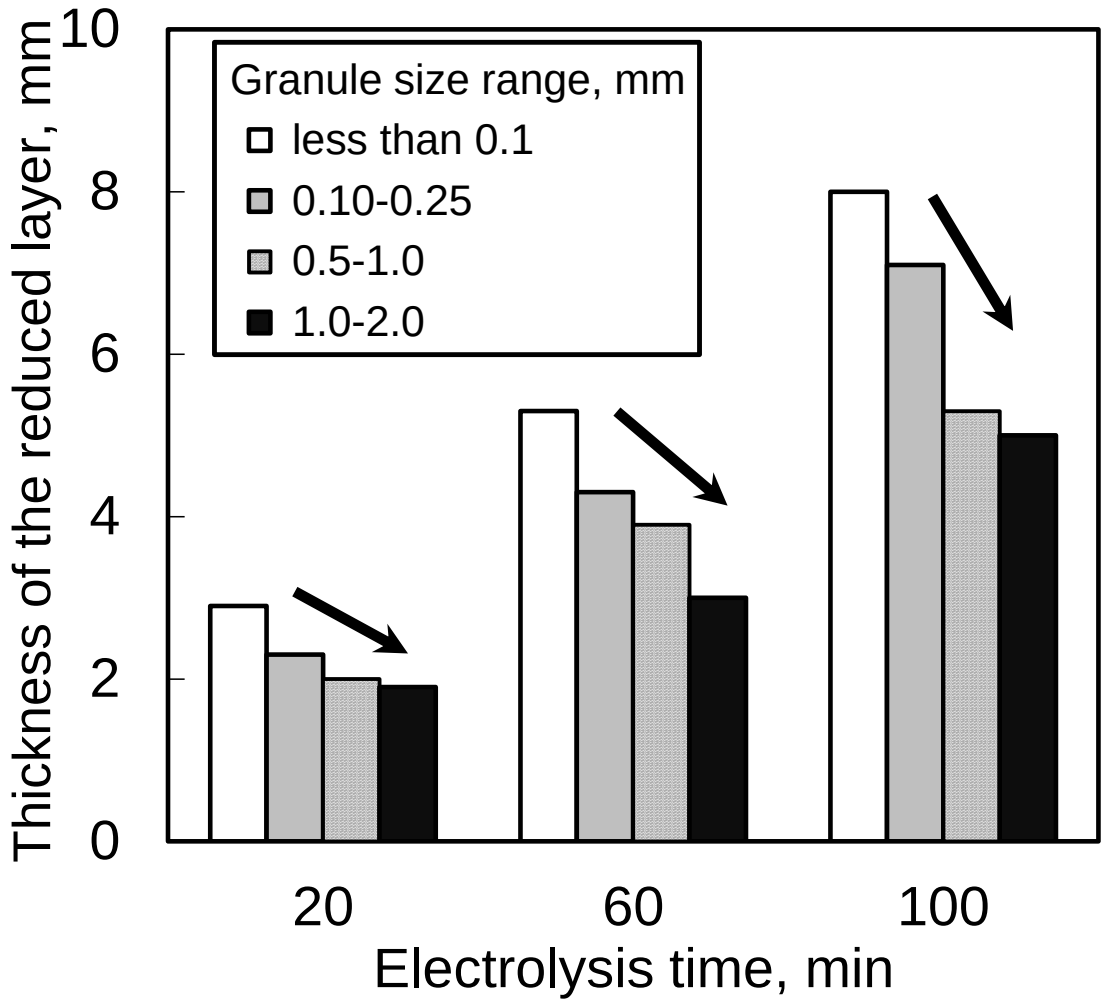

Figure 5—Thickness of the reduced layers after electrolysis for 20, 60 and 100 min using SiO_2 granules with different size ranges at 0.5 V vs. Ca^{2+}/Ca in molten $CaCl_2$ at 1123 K (850 ℃).

Yang et al.

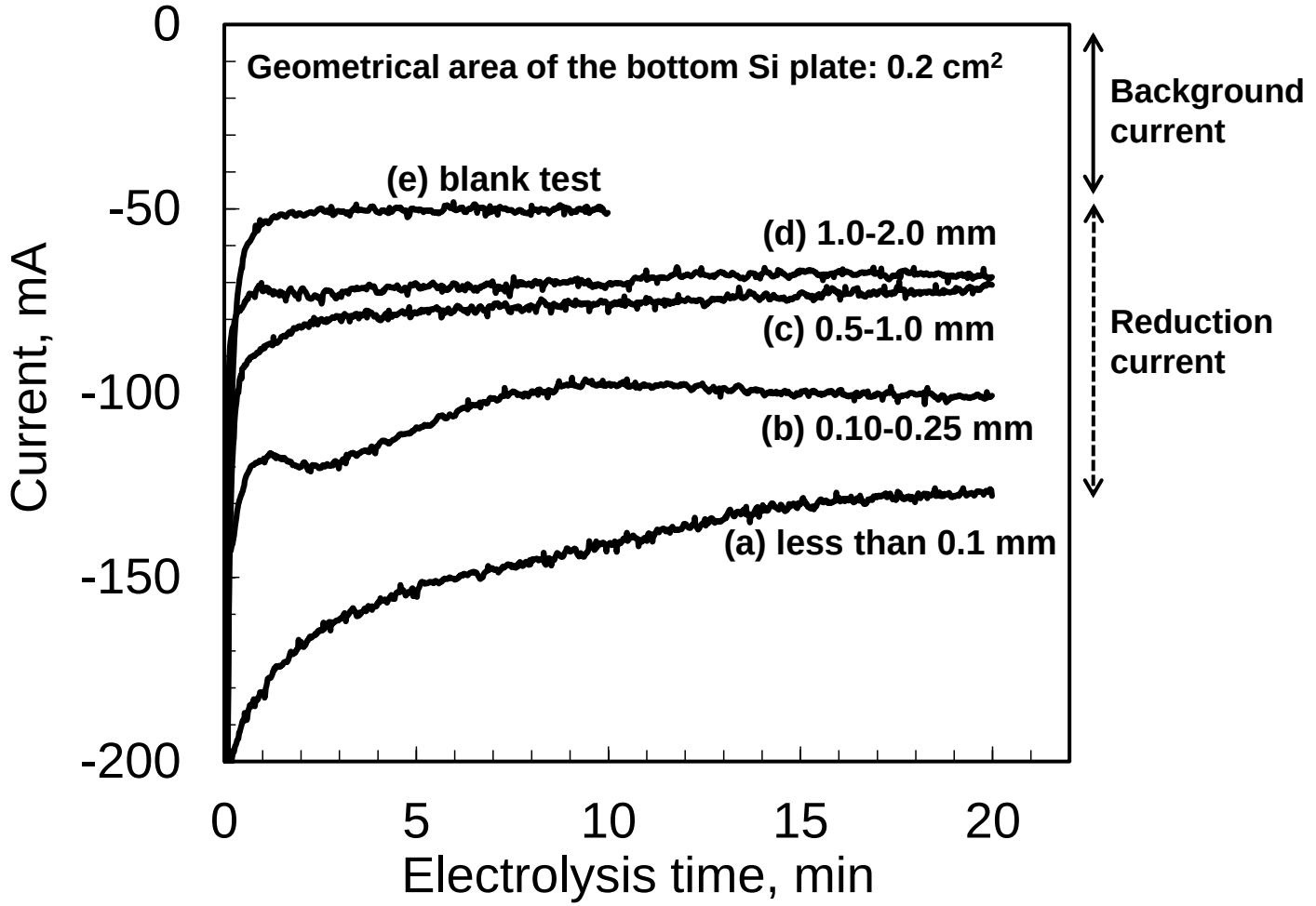

Figure 6—Current transient curves during electrolysis using SiO_2 granules with size ranges of (a) less than 0.1 mm, (b) 0.10–0.25 mm, (c) 0.5–1.0 mm and (d) 1.0–2.0 mm for 20 min and (e) during a blank electrolysis test for 10 min at 0.5 V vs. Ca^{2+}/Ca in molten $CaCl_2$ at 1123 K (850 ℃).

Yang et al.

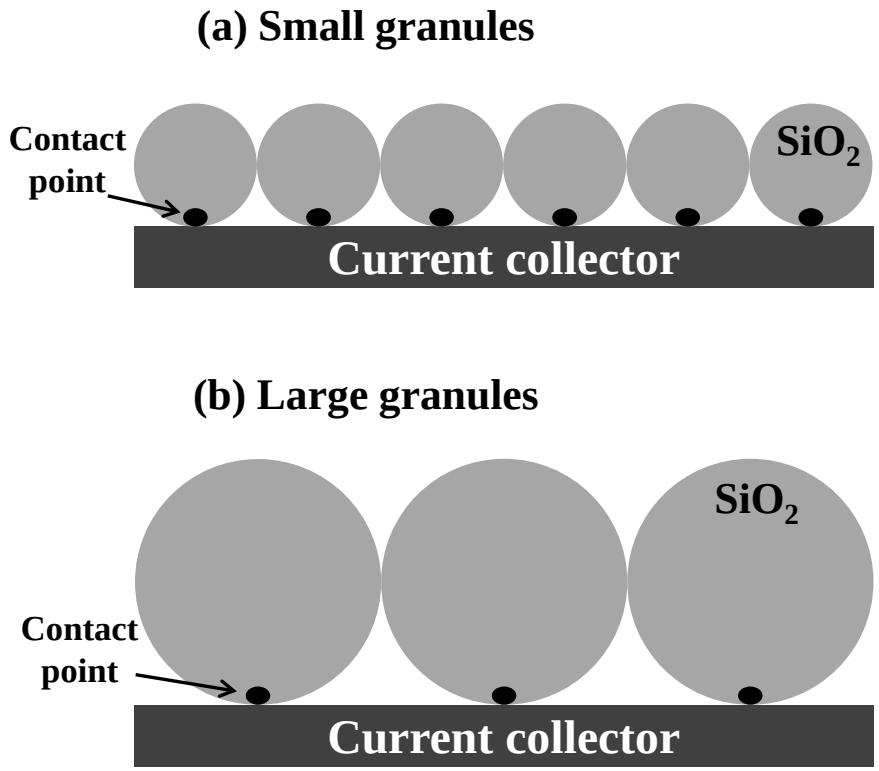

Figure 7—Schematics of the contact between SiO_2 granules and the bottom current collector (Si plate).

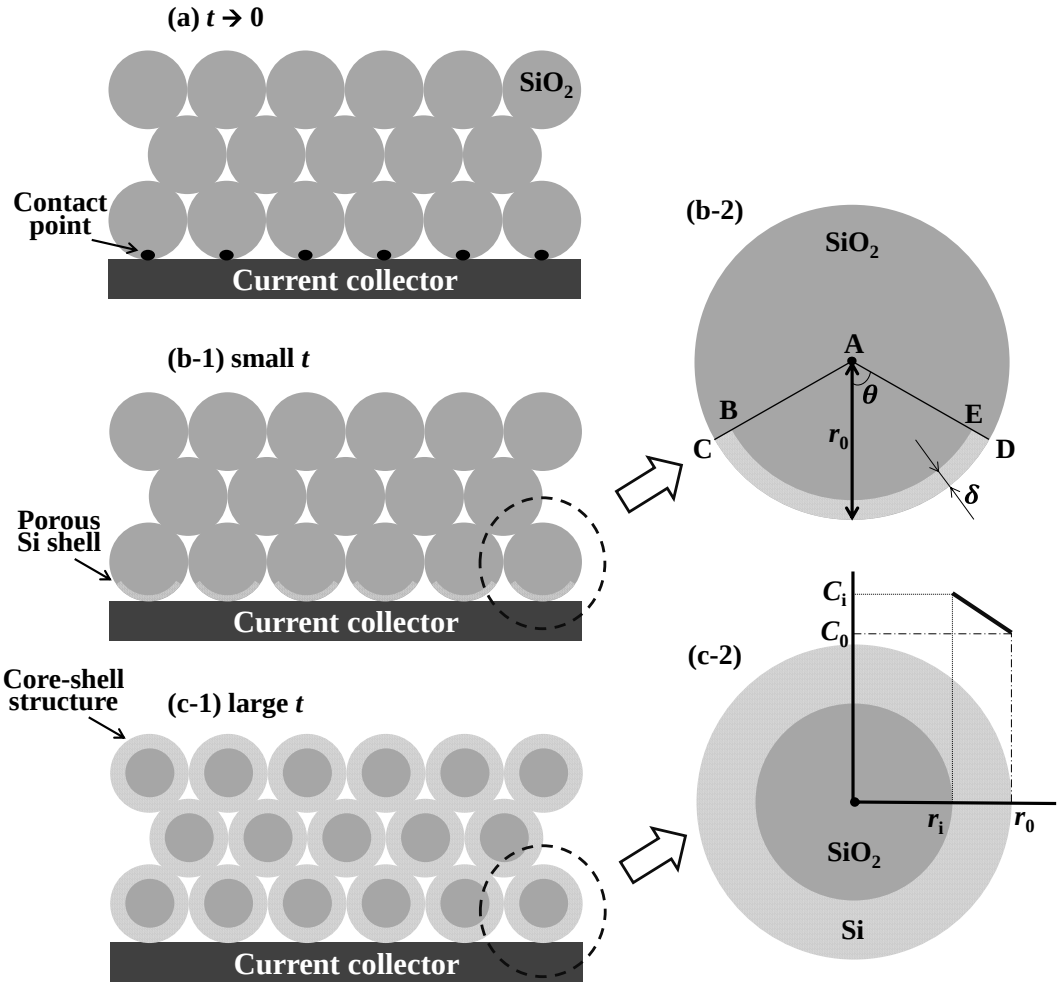

Figure 8—Schematics of the reduction of the SiO_2 granules during electrolysis.

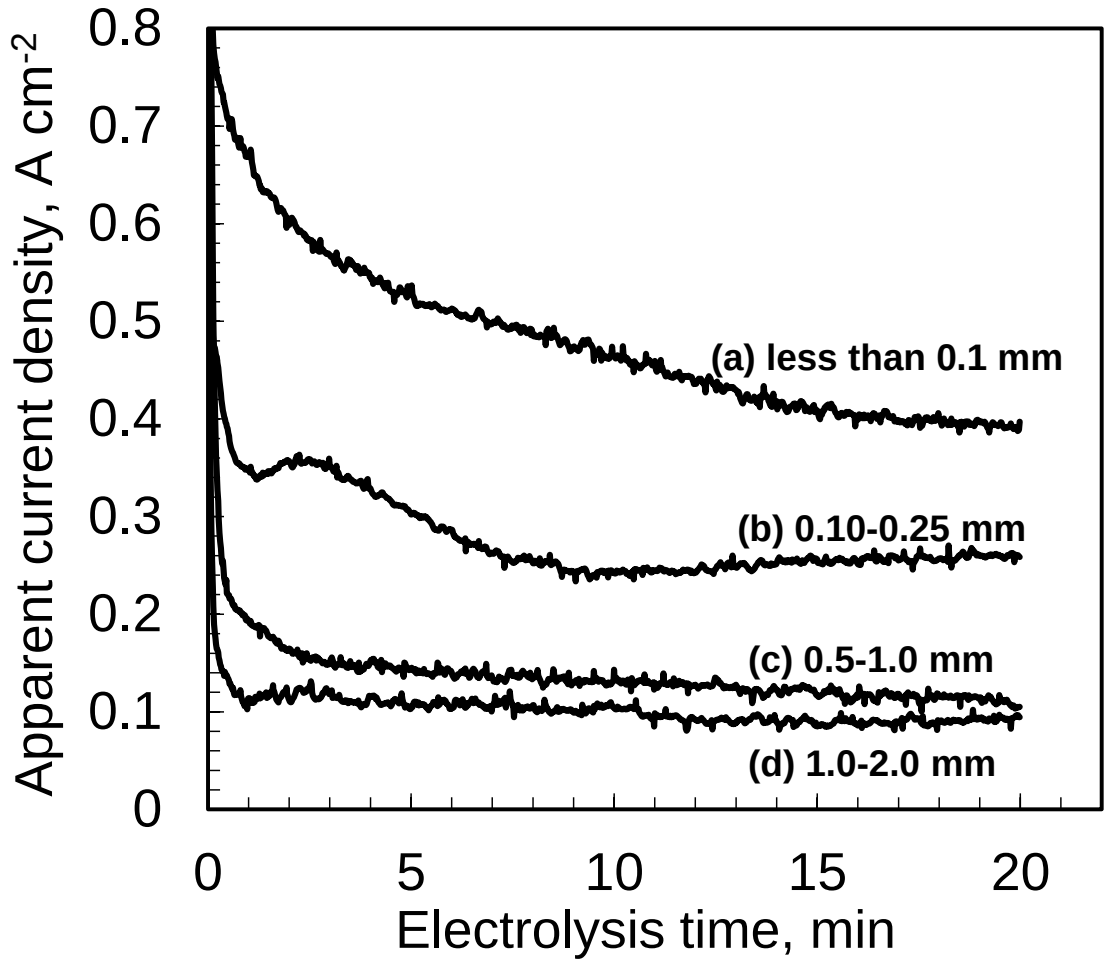

Figure 9—Variation of apparent current density during electrolysis within 20 min using SiO_2 granules with size ranges of (a) less than 0.1 mm, (b) 0.10–0.25 mm, (c) 0.5–1.0 mm and (d) 1.0–2.0 mm at 0.5 V vs. Ca^{2+}/Ca in molten $CaCl_2$ at 1123 K (850 ℃).

Yang et al.